Defect-enhanced Rashba spin-polarized currents in carbon nanotubes

Hernán Santos,[1,2] Leonor Chico,[3] J. E. Alvarellos,[1] and A. Latgé[2,*]

[1] *Dep. de Física Fundamental, Universidad Nacional de Educación a Distancia, Apartado 60141, E-28040 Madrid, Spain*
[2] *Instituto de Física, Universidade Federal Fluminense, Niterói, Av. Litorânea sn 24210-340, RJ-Brazil*
[3] *Instituto de Ciencia de Materiales de Madrid, Consejo Superior de Investigaciones Científicas, C/ Sor Juana Inés de la Cruz 3, 28049 Madrid, Spain*

(Dated: August 30, 2022)

The production of spin-polarized currents in pristine carbon nanotubes with Rashba spin-orbit interaction has been shown to be very sensitive to the symmetry of the tubes and the geometry of the setup. Here we analyze the role of defects on the spin quantum conductances of metallic carbon nanotubes due to an external electric field. We show that localized defects, such as adsorbed hydrogen atoms or pentagon-heptagon pairs, increase the Rashba spin-polarized current. Moreover, this enhancement takes place for energies closer to the Fermi energy as compared to the response of pristine tubes. Such increment can be even larger when several equally spaced defects are introduced in the system. We explore different arrangements of defects, showing that for certain geometries there are flips of the spin-polarized current and even transport suppression. Our results indicate that spin valve devices at the nanoscale may be achieved via defect engineering in carbon nanotubes.

PACS numbers: 73.63.-b, 72.25-b

arXiv:1707.00642v1 [cond-mat.mes-hall] 30 Jun 2017

I. INTRODUCTION

The departure from ideal crystalline order in carbon materials with sp^2 hybridization, due the presence of topological defects, lattice distortions or atomic adsorption, has strong consequences in the physical properties of such nanosystems [1]. In particular, these defects can create magnetic moments, as it has been observed in graphene by means of spin currents [2] or scanning tunneling microscopes [3]. Novel control and manipulation features of these microscopes [3, 4] and advances in material growth techniques [5, 6] are the basis of outstanding experimental results. Some of them make possible the generation of topological defects in specific lattice positions [4], while others allow for the control of the lattice structure, size and other structural properties of material. Typical examples are the chirality and radius of carbon nanotubes (CNTs) [5], or the width and the edge shape of graphene nanoribbons [6].

The prediction of spin-polarized currents induced by Rashba spin-orbit (RSO) interaction in carbon materials has been recently made [7, 8], even in the absence of external magnetic fields or magnetic impurities. These results indicate the possibility of achieving stable spin-polarized electrical currents from unpolarized charge currents, paving the way toward the creation of carbon-based spin valve devices at the nanoscale. Such studies focussed on ideal pristine systems, but the role of defects in carbon materials under a RSO interaction has not yet been addressed.

Vacancies, adsorption of hydrogen atoms, and defects in general act as localized perturbations in graphene systems and can induce localized states close to the Dirac point. The effects of such perturbations on the electronic properties of the system are greatly dependent on their position in the two sublattices of graphene and carbon nanotubes [9–12]. When a p_z orbital is removed from one sublattice of pristine graphene, due for instance to the creation of a vacancy, a new state appears on the other sublattice, localized around the perturbation [13]. Hydrogen adatoms also produce such localization effects; indeed, if we are not interested in the analysis of the resulting magnetic moments, we may consider both situations as equivalent.

The aim of the present work is to investigate how defected CNTs under external electric fields may produce spin-polarized currents due to RSO coupling, opening up novel routes for engineering the spin-dependent transport response on CNTs. We explore the possibility of enhancing such spin-polarized currents in CNTs [8] in the presence of topological defects or hydrogen adatoms (H-adatoms). We will focus on the effects of the particular positions of such defects and their spatial distribution on the spin-polarized currents, and the energy ranges at which spin-polarized conductances appear. We show that the introduction of defects permits the appearance of spin-polarized currents closer to the Fermi level of the pristine systems.

The article is organized as follows: In Sec. II we describe the systems, model and methods that we use to obtain the spin transport properties under a RSO interaction. Sec. III deals with the emergent effects of isolated vacancies or defects on the transport properties, the enhancement of spin-polarized currents due to multiple defects and the polarized-current dependence on the relative orientation of defects; finally, the interplay of RSO interaction and the effects of random H-adatoms are explored. In Sec. IV we present the conclusions of the paper.

* andrea.latge@gmail.com

II. SYSTEM AND MODEL

A. Description of the system

To analyze the effects of localized defects on the spin-polarized currents generated by Rashba spin-orbit interactions, we propose a device made of a CNT that has a region of length L placed between two metallic plates with an uniform electric field $\boldsymbol{\mathcal{E}}$ between them (see Fig. 1(a)). As we are interested in transport properties, we concentrate in metallic nanotubes, and restrict the study to armchair (n, n) tubes. The central part under the applied electric field has an induced Rashba spin-orbit (RSO) interaction; we name it the *Rashba region*. Notice that the system may be described as an infinite carbon nanotube with three parts: a central finite Rashba region connected to two semiinfinite nanotube leads of the same chirality and radius [8]. The length L of the Rashba region can be given in terms of the length T of the translational vector by $L = NT$ (with $N \in \mathbb{N}$) [14]. Recall that $T = \sqrt{3}a_c$ for armchair tubes, where a_c is the carbon bond length in graphene.

We introduce defects in this Rashba region. Specifically, as depicted in Fig. 1, we have chosen H-adatoms, shown in (b), and 5-7-7-5 Stone-Wales defects (i. e., two carbon pentagon-heptagon pairs placed antiparallel to each other), rendered in (c). The carbon atoms in which the defects produce important changes in the density of states are highlighted in red, being 12 atoms for the H-adatom and 16 for the SW defect.

The presence of H-adatoms does not mix the two CNT sublattices, although depending on their number and position, they may break sublattice symmetry, allowing the appearance of localized magnetic moments on the atoms close to the H-adatoms [11].

On the other hand, the introduction of topological defects in the hexagonal lattice of graphene or CNTs with an odd-number of carbon atom rings mixes the two sublattices. Additionally, the combination of the two most probable topological defects, a single 5-7 (pentagon-heptagon) pair in a carbon nanotube changes its chirality [15, 16]. However, two adjacent 5-7 pairs in opposite direction, the 5-7-7-5 Stone-Wales (SW) defect, preserves the chirality of the CNT, but there is still a local sublattice mixing. With the aim to simplify the analysis, we will focus only on defects that preserve the chirality, and so we will study the effects of the RSO interaction on CNTs with H-adatoms and SW defects.

B. Model and method

Our calculation employs a single-orbital tight-binding model in the nearest-neighbor approximation with a RSO coupling limited to the central part of the carbon system [7, 8, 17, 18]. The Hamiltonian can be written

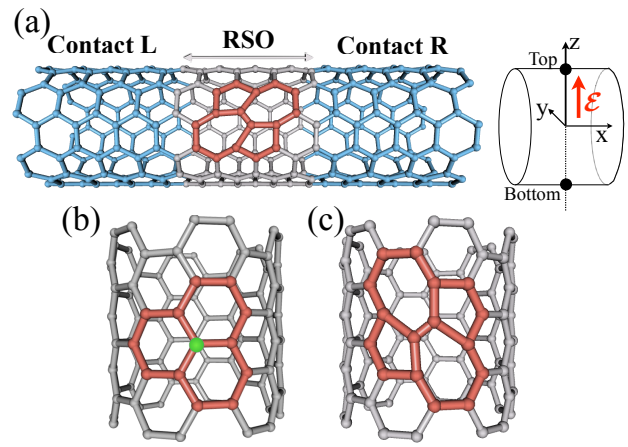

FIG. 1. (Color online) (a) Schematic view of the device geometry. Left (L) and right (R) contacts are pristine CNTs without RSO interaction. The central part of the device is a conducting CNT of length L, with RSO interaction induced by the presence of an uniform electric field $\boldsymbol{\mathcal{E}}$ in the z direction (red arrow). The directions x, y and z are shown in the right part of the figure; the electric field points into the $+z$ direction. The top and bottom locations of the CNT are defined with respect to the electric field, as indicated. Examples of the defects considered (highlighted in red): (b) a H-adatom, shown in green on top of a carbon atom, and (c) a Stone-Wales topological defect.

as $H = H_0 + H_R$, with the kinetic energy term being $H_0 = -\gamma_0 \sum c^\dagger_{i\alpha} c_{j\alpha}$, where $c^\dagger_{i\alpha}$ ($c_{j\alpha}$) is the creation (destruction) operator for electrons with spin projection α in site i (j), and γ_0 is the nearest-neighbor hopping energy, which is constant throughout the system. This amounts to neglect the lattice relaxation produced by the defects, but this is a quantitative change with respect to lattice imbalance and mixing or orbital removal.

The RSO contribution to the Hamiltonian is

$$H_R = \frac{i\lambda_R}{a_c} \sum_{\substack{<i,j> \\ \alpha,\beta}} c^\dagger_{i\alpha} \Big[(\boldsymbol{\sigma} \times \mathbf{d}_{ij}) \cdot \mathbf{e}_z \Big]_{\alpha\beta} c_{j\beta} \ , \qquad (1)$$

where $\boldsymbol{\sigma}$ are the Pauli spin matrices, $\mathbf{d}_{ij}$ is the position vector between sites i and j, and α, β are the spin projection indices. The unit vector $\mathbf{e}_z$ is along the electric field $\boldsymbol{\mathcal{E}}$ direction. The Rashba spin-orbit strength λ_R is given by the electric field intensity, and its sign defined by the field orientation. A value of $\lambda_R = 0.1\gamma_0$ is used [7, 8]. Although this value is very large with respect to the intrinsic spin-orbit interaction of a pristine carbon nanotube, the enhancements reported for functionalized and decorated graphene systems [19, 20] demonstrate that similar values may be achieved in defected carbon tubes.

As previously discussed [8], the direction for which the spin-polarized current is largest is that perpendicular to both the current and the external electric field; in our case it corresponds to the y-direction. This fact can be best understood by resorting to the expression of the Rashba term in the continuum approximation [21], i. e,

$H_R \propto (\boldsymbol{\sigma} \times \mathbf{k}) \cdot \boldsymbol{\mathcal{E}}$, with $\mathbf{k}$ being the wave vector which is in the direction of the current.

The conductance along the nanotube axis (x direction) is calculated following the Landauer approach in the zero bias approximation [8, 15]. Assuming unpolarized charge currents flowing from left to right, the spin-dependent conductance $G^{LR}_{\sigma\sigma'}(E)$ is proportional to the probability that an electron with spin σ and energy E in the left contact reaches right contact with spin σ'. This probability can be calculated using the Green function formalism [22, 23]. The spin polarization of the conductance in the y-direction is defined as

$$P_y(E) = G^{LR}_{\sigma\sigma} - G^{LR}_{\sigma\bar{\sigma}} + G^{LR}_{\bar{\sigma}\sigma} - G^{LR}_{\bar{\sigma}\bar{\sigma}} \,, \qquad (2)$$

where $\bar{\sigma}$ means $-\sigma$. As already mentioned, we restrict ourselves to the y-direction for the spin projections. In the small-bias limit, this magnitude is proportional to the y-component of the spin current. Although other authors employ a normalized adimensional spin-polarization factor [23, 24], we have chosen this definition which is directly related to the spin-dependent conductances $G^{LR}_{\sigma\sigma'}(E)$.

III. RESULTS

We consider an infinite metallic $(6, 6)$ armchair CNT with a central finite Rashba region of varying length L, that it is given in terms of the length T of the translational vector, NT. We will study Rashba regions with varying density of defects, and we also investigate the optimum condition for the relative orientation between the defects and the electric field direction. The Rashba region will have a number M of H-adatoms or SW defects. We assume that an unpolarized current flows from the left semiinfinite nanotube through the Rashba region towards the right end. In Ref. [8] we have shown that, for a pristine CNT, spin scattering in the Rashba region generates spin-polarized currents for certain spin directions and system symmetries. Here we analyze the effect of localized defects on the spin-polarized currents traversing the Rashba region.

As commented, we have focused on the analysis of the spin-projected conductance along the direction (y) perpendicular to both the current (x) and the external electric field (z) directions, since it exhibits the largest spin-polarized current. In particular, we get null spin polarizations P_z and P_x for all the armchair nanotubes (n, n) with even n index for symmetry reasons [8]. In contrast, the spin polarization is maximized in the y direction, for which there are no symmetry restrictions for its occurrence.

A. Single defects

Spin-polarized conductances are evaluated for different sizes of the Rashba region, considering first the case of a single defect on the top position. Recall that we took the electric field direction to be the $+z$, and the $x-$direction along the nanotube axis. We orient the nanotube so that the H-adatom is situated on the $+z$ axis and the flux of the electric field through the area enclosed by the red highlighted bonds in Fig.1(b) is maximum. For the SW defect, we proceed likewise, taking the $+z$ axis passing through the middle point of the bond between the two adjacent heptagons in Fig.1(c). Note that both top and bottom positions give the maximal flux of the electric field $\boldsymbol{\mathcal{E}}$ (in absolute value) through these defects.

Panels (a) and (b) of Fig. 2 present the results of the P_y-spin polarization for the pristine case and for the single defect case (*case 1*), using a Rashba region length $L_0 = 9T \approx 2.21$ nm, both for the H-adatom and the SW defect. Notice that for the pristine case, there are not spin-polarized conductances for energies close to the Fermi level, even though there are two channels available for the conductance related to the two different valleys [24]. This is due to the lack of scattering processes in the Rashba region between states in different K valleys when the sole perturbation is the electric field [8, 25]. But for energies close to $E = \pm 0.52\gamma_0$ the spin-polarized conductance P_y presents two peaks, allowed by the opening of other conductance channels in the nanotube contacts [8]. However, when a single defect (H-adatom or SW defect) is added to the Rashba region, intervalley scattering is allowed. But the effect, as shown in Figs. 2 (a) and (b), is too small to be noticeable for energies close to the Fermi level. These results for single defects are almost indistinguishable for the case of the H-adatom, whereas for the SW defect we observe small differences around peaks at $E = \pm 0.52\gamma_0$ (see *case 1* in panels (a) and (b) of Fig. 2). Thus, when only one scattering center is considered in the Rashba region, the RSO effect close to the Fermi level is not easily distinguishable from the pristine case.

B. Multiple defects

In contrast to the single defect case, when we consider several M equidistant defects at the top position of the Rashba region, the spin-polarized conductance becomes significant close to the Fermi level. We choose different Rashba regions composed of M $(6, 6)$ finite CNT portions, each of them with a length L_0 and with a H-adatom or a SW defect in it. The defect density is kept constant, i.e., one defect per length L_0. The top panels of Fig. 2 [(a) and (b)] show the spin polarization of the conductance P_y for the cases $M = 1, 2, 3, 4$. The heights of the maxima with energies within the first conductance plateau range of the pristine CNT increase with the number of defects. Similarly to the pristine CNT described by a single p_z orbital tight-binding Hamiltonian, for the nanotube with H-adatoms P_y shows electron-hole symmetry, $P_y(E) = -P_y(-E)$. This symmetry is bro-

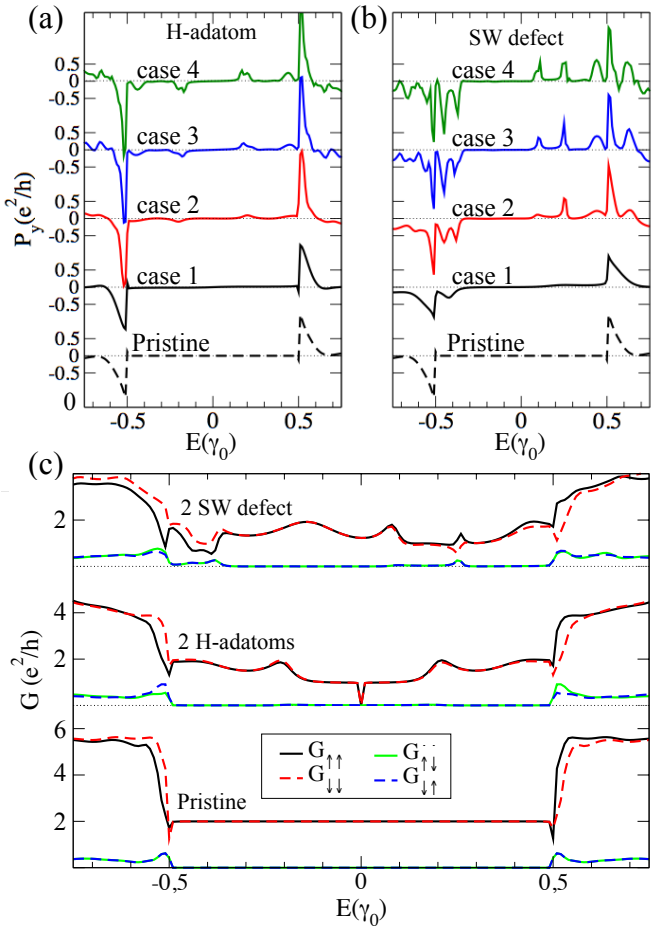

FIG. 2. (Color online) Armchair (6, 6) CNTs with a Rashba region with different lengths and number of defects. Panels (a) and (b): P_y-spin polarization. Each *case* M corresponds to Rashba regions composed of M finite CNT portions, each with a length $L_0 = 9T$ and with a H-adatom or a SW defect. Panel (c): Spin-dependent conductances for a Rashba region $L = 2L_0 = 18T \approx 4.43$ nm. Low, middle, and up curves correspond to a pristine tube, two H-adatoms, and two SW defects equally spaced in the Rashba region, respectively.

ken when topological SW defects are considered in the Rashba region (panel (b)).

The bottom panel, Fig. 2 (c), represents the spin-dependent conductance as a function of the energy for the original pristine tube and the case $M = 2$. Close to the Fermi energy, the presence of the two defects, either H-adatoms or SW defects, is evident for the spin-dependent conductances $G_{\uparrow\uparrow}$ and $G_{\downarrow\downarrow}$, being negligible for the spin-flip conductances $G_{\uparrow\downarrow}$ and $G_{\downarrow\uparrow}$.

For the nanotube with two H-adatoms, the spin polarization close to the Fermi energy exhibits small peaks at energies $E = \pm 0.21\gamma_0$. The peaks coincide with the enhancement of the spin-dependent conductances $G_{\sigma\sigma}$ from e^2/h to $2e^2/h$, due to the electronic states localized around the adatoms [8]. This effect is more remarkable as the number of equally spaced adatoms in the Rashba region increases, as shown in Fig. 2 (a) (*cases 3* and *4*).

More relevant changes in the spin-polarized currents appear for the SW defects, as also shown in Fig. 2 (b). Two peaks can be seen at energies $E = 0.09\gamma_0$ and $0.25\gamma_0$ in the case of two defects (*case 2*); these peaks are even higher for larger number of defects (*cases 3* and *4*). On the other hand, for energies around $E = \pm 0.5\gamma_0$ (i.e., close to the transition from the first to the second conductance plateau range of the pristine CNT) the P_y exhibits much more features than the H-adatom defect configuration. Due to sublattice mixing, the electron-hole symmetry is broken for the SW defected tubes, yielding a strong asymmetry in the results.

Band structure and spin analysis

To understand the effect of the H-adatoms and the SW defects in the spin-polarized currents induced by the Rashba SOI, we resort to the analysis of the band structure and the spin-polarization of an infinite periodic system, choosing a CNT unit cell of length L_0 with a single H-adatom or one SW defect in it. The RSO interaction is present in the whole system.

Panels (a) of Fig. 3 presents the band structures for the (6, 6) CNT with Rashba SOI, with either H-adatoms (upper panel) or SW defects (bottom panel). The expectation values for the y-spin component, $\langle S_y \rangle$, projected in all the atoms around the defect or belonging to it (highlighted in red in Fig. 1), are shown as a color scale in the bands.

The expectation value of the spin at a specific atom n is given by $\langle S_y \rangle_n = \frac{\hbar}{2}\langle \sigma_y \rangle_n$, with $\langle \sigma_y \rangle_n = \langle \phi_n | \sigma_y | \phi_n \rangle$, where ϕ_n is the tight-binding atomic eigenfunction in the single-orbital model. We have also plotted in Fig. 3 a zoom of the band structure in the relevant energy range (in panels (b)) as well as the corresponding P_y-spin polarizations (in panels (c)).

For the H-adatom, bands with large absolute values of $\langle S_y \rangle$ appear in the energy range from $E \approx \pm 0.16\gamma_0$ to $E \approx \pm 0.22\gamma_0$, coinciding with the bumps that appear in the spin-polarization conductance P_y in Fig. 2(a) (with L up to $4L_0$, where $L_0 = 9T \approx 2.21$ nm) and shown much more clearly in Fig. 3(c), top panel (obtained for a system with $L = 20L_0$). Recall that for current flowing from left to right, the states that contribute to the current scattering process are those with positive velocity [26, 27]. The band structure in the range from E= $0.16\,\gamma_0$ to E= $0.19\,\gamma_0$ shows a band from $\mathbf{k} = 0.25\,\overline{\Gamma X}$ to $\mathbf{k} = 0.40\,\overline{\Gamma X}$ with a strong positive $\langle S_y \rangle$ spin, however, there is no band with negative $\langle S_y \rangle$ spin, due to the gap open around Γ by the strong band hybridization, see the zoom in Fig. 3(b), top panel. At the same energy range P_y shows a positive peak (Fig. 3(c), top). Nevertheless, in the energy range from $0.195\,\gamma_0$ to $0.21\,\gamma_0$, P_y shows a negative peak, because the band with positive slope in

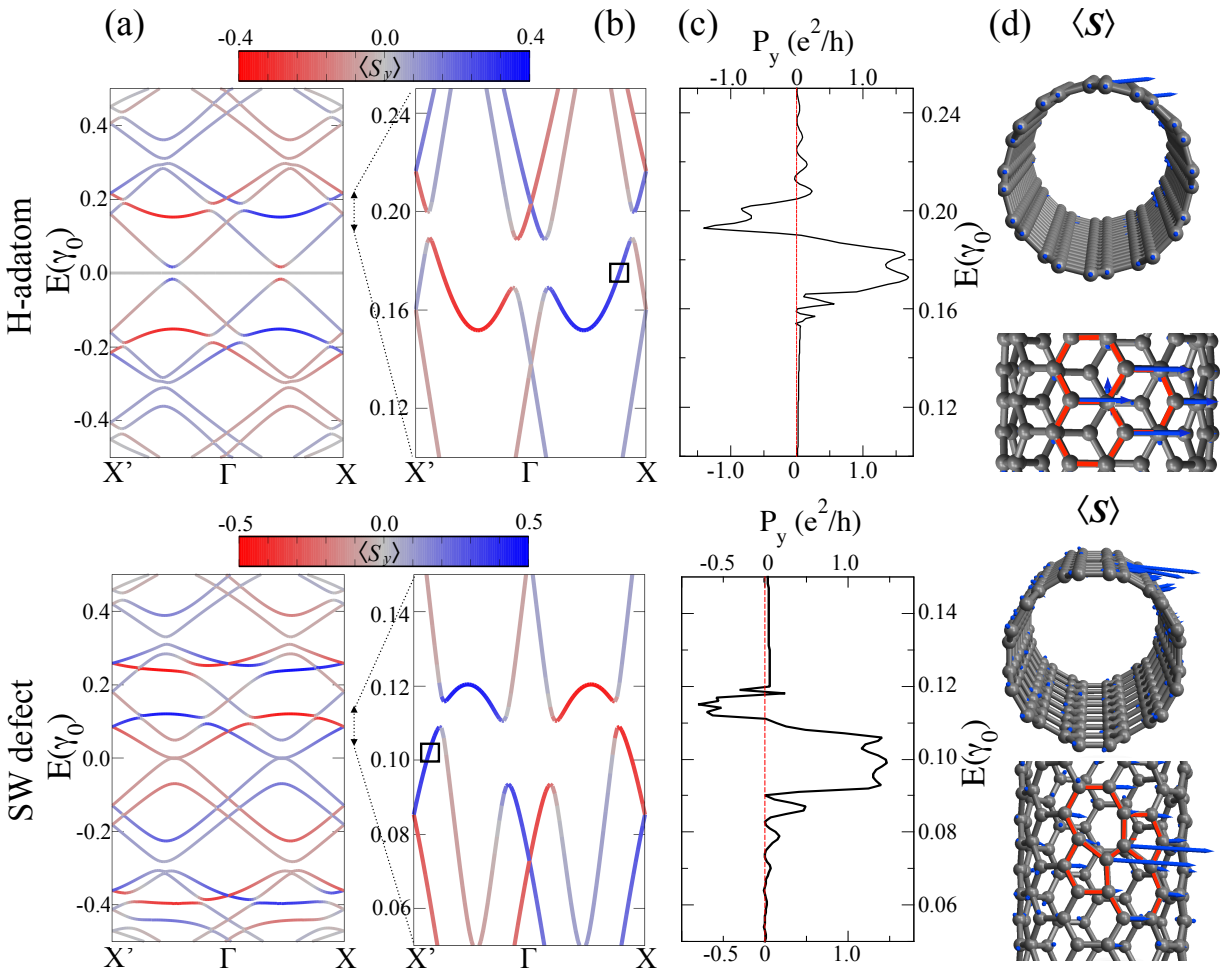

FIG. 3. (Color online) Results for the defected (6, 6) CNTs (with H-adatoms or with SW defects) under the RSO interaction. Panels (a): Band structures of infinite defected (6, 6) CNTs composed of finite nanotube stacks (each of a length $L_0 = 9T$ and with one defect). Zooms of the band structures in the relevant energy range are shown in the panels (b). The spin values of the $\langle S_y \rangle$ at the adatoms and SW defects, as defined in Fig. 1, are presented in color resolution (blue for up spin and red for down spin). Panels (c): The corresponding P_y-polarization conductances are shown for $L = 20\,L_0$, where $L_0 = 9T \approx 2.21$ nm. Panels (d): Lateral schematic view of the defected tube with a H-adatom and with a SW defect. Blue arrows denote $\langle \mathbf{S} \rangle$ values at atoms in the defect for the k values highlighted with black squares in panels (b).

that energy interval has negative values of $\langle S_y \rangle$ (red color in the bands of Fig. 3). A similar enhancement of the spin-polarization P_y is also found when a higher number of defects in the Rashba region (with the same defect density) is considered. The small peak intensity found at this energy for $L = 2L_0$ in Fig. 2 (a) clearly increases with the length and the number of defects (i.e. for *cases 3* and *4*). Taking into account the electronic band features shown for the periodic defected CNT (Fig. 3), we conclude that the peaks on the spin-polarization currents around $E \approx \pm 0.2\ \gamma_0$ are actually associated to the existence of equally spaced adatoms in the Rashba region. Besides the spin polarization of the bands, the opening of gaps at certain wavevectors produces an imbalance between the chanells with opposite values of the spin projection, giving rise to spin-polarized currents. Moreover, in Fig. 4 we present the results for 20 H-adatoms on the top A positions, equally spaced on a Rashba region with a length of $20\,L_0$ and $L_0 = 4T$, showing quite similar peaks at the same energy ranges.

For the case of a SW defect, we show the band structure and its $\langle S_y \rangle$ values in the bottom panel of Fig. 3 (a). The energy ranges presenting large absolute values of $\langle S_y \rangle$ at the defect occur approximately from $0.08\,\gamma_0$ to $0.12\,\gamma_0$ and from $0.24\,\gamma_0$ to $0.26\,\gamma_0$. As in the H-adatom case, the spin polarized current appears when there is an inequality between the channels with opposite values of $\langle S_y \rangle$ due to the band opening. These energy ranges coincide with the P_y enhancement presented in Fig. 2(b), that also happens in the results shown in Fig. 5.

We plot in Figs. 3 (d) the spin $\langle \mathbf{S} \rangle$ corresponding to the states which give rise to the polarized current, with k values marked by black squares in the zooms shown in Figs. 3 (b). This expectation value is projected on each

atom n, $\langle \mathbf{S} \rangle_n = \langle S_x \rangle_n \, \mathbf{e}_x + \langle S_y \rangle_n \, \mathbf{e}_y + \langle S_z \rangle_n \, \mathbf{e}_z$, where $\langle S_i \rangle_n = \frac{\hbar}{2} \langle \sigma_i \rangle_n$, $i = x, y, z$, and $\langle \sigma_i \rangle_n = \langle \phi_n | \sigma_i | \phi_n \rangle$. Their energies and wavevectors are $E = 0.173\,\gamma_0$ and $\mathbf{k} = 0.375\ \overline{\Gamma \mathrm{X}}$ for the H-adatom and $E = 0.1065\,\gamma_0$ and $\mathbf{k} = 0.41\ \overline{\Gamma \mathrm{X}'}$ for the SW defect. The large absolute values of $\langle \mathbf{S} \rangle$ in those bands, related to the high spin-polarized current values in Fig. 3 (c), are located around the defects. They also show larger values in the three nearest-neighbors of the carbon atom with the adsorbed hydrogen, and at the boundary atoms belonging to both the 7- and 5-rings of the SW defect. Therefore, when compared with the pristine CNT results [8], we see that the spin polarization $\langle S_y \rangle$ of these states, plus the gap opening due to band hybridization, are responsible for the spin-polarized conductance peaks that now appear close to the Fermi energy. This is also true for other states: for the SW defects the spin values $\langle S_y \rangle$ of the electronic states of the bands with positive slope presented in color resolution in Fig. 3 (a, bottom), plus the gaps open at Γ, are clearly related to the P_y structures that appear in Fig. 2 (b) around energies $\pm 0.5\,\gamma_0$.

C. Influence of the relative alignment of defects and the electric field

We analyze now the dependence of the spin-polarized currents on the relative position of the defect in the original tube with respect to the electric field direction. We consider a (6,6) CNT with a Rashba region composed of 20 L_0 with their corresponding adatoms equally spaced. In this case we use $L_0 = 4\,T$, representing a sample with higher concentrations of defects within the Rashba area. By fixing the electric field in the $z-$direction, we vary the relative orientation of all the defects from the parallel direction with respect to the field (top position, labeled A in Figs. 4 and 5) to the perpendicular direction (lateral tube side, labeled G), through intermediate defect positions in the tube. In Fig. 4 we present the results of the spin-polarization P_y of the conductance for the H-adatom case, considering the relative positions in the tube shown in the inset of the figure. The H-adatom-induced peaks of P_y close to the Fermi energy can be seen, continuously decreasing in intensity as the H-adatom positions change from A to G, with a sharp reduction of P_y from F to G. This is highlighted in the inset (lower part of Fig. 4) that shows the dependence of the maximum value of P_y on the angle between the vector position of the adatoms and the electric field. This effect can be expected from the expression of the Rashba Hamiltonian: at position A, the vectors defining the bonds in the defects are perpendicular to $\boldsymbol{\mathcal{E}}$, maximizing their contribution to the Rashba term, whereas for position G the electric field is contained in the plane formed by these bonds, yielding a much smaller contribution. As commented, the electric flux of $\boldsymbol{\mathcal{E}}$ through the defects is maximal when the defects are at the top or the bottom positions on the nanotube. Therefore, the effect of the RSO is maximized for a maximum flux of the electric field through the defects.

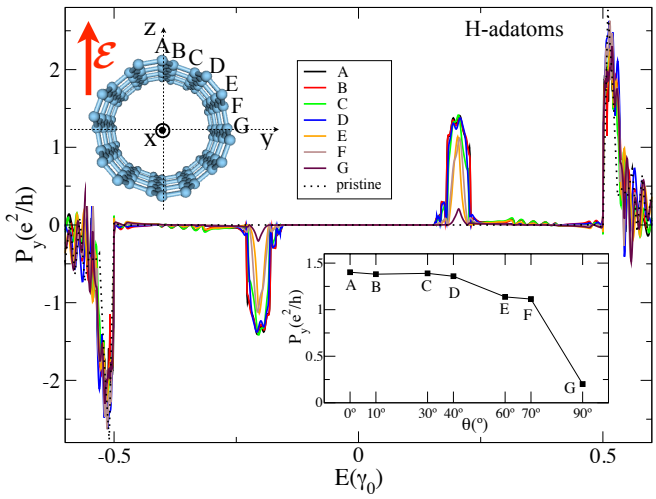

FIG. 4. (Color online) Spin-polarization of the conductance, P_y, for a $(6,6)$ CNT with a Rashba region composed of 20 H-adatoms equally spaced in a length given by $20\,L_0$ ($L_0 = 4T \approx 0.98$ nm), for different positions of the adatom relative to the electric field direction. Position A corresponds to all the H-adatoms placed at the top of the tube, whereas G when the adatoms are situated at the side of the tube. Intermediate cases (B to F) are also investigated. All H-adatom configurations are graphically detailed in the CNT scheme at the top inset.

Similar results have been found for the SW defects. Fig. 5 shows P_y for three relative orientation of the defects in the tube with respect to the electric field direction, indicated in the inset of the figure (positions A, D and G). The same defect density and length of the Rashba region employed for the H-adatoms are used here for the SW defects. Going from A to G, two noticeable effects can be remarked. Firstly, a big decrease of the P_y values for the peak close to $E = -0.14\,\gamma_0$. In fact, the height of the peak of P_y at this energy when the defects are located at G (the lateral side of the tube) is only about 30% the value obtained for the top position A. Secondly, a pronounced narrowing of the width of the peak that appears in the energy range between $E = 0.1\,\gamma_0$ and $0.18\,\gamma_0$. As expected, the relative position of the defects with respect to the electric field plays again an important role in the spin-polarized conductances.

In order to investigate the effects of the relative positions between the defects, we further consider the case of two H-adatoms in the unit length L_0, taking a Rashba region length equal to $20\,L_0$, where L_0 is now $L_0 = 9\,T$. In case 1 two H-adatoms are placed both at the top of the tube. In case 2 the position of one H-adatom is at the

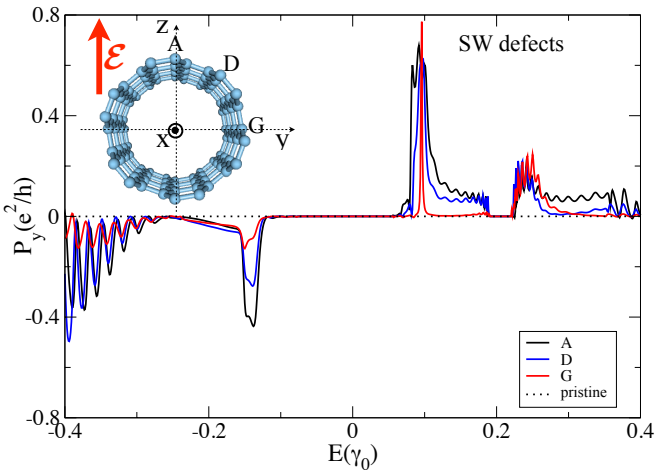

FIG. 5. (Color online) Spin polarization of the conductance, P_y, for a $(6,6)$ CNT with a Rashba region length equal to $20\,L_0$ ($L_0 = 4T \approx 0.98$ nm), with 20 SW defects inside, for different positions of the defects with respect to the electric field. Position A corresponds to all the defects located at the top of the tube, G when they are situated at the nanotube side and D is an intermediate case. All the three cases are detailed in the CNT scheme at the top inset.

top and the other at the tube bottom, but not in diametrically opposite sites of the tube. Configuration 3 is the most symmetric case; one H-adatom in front of the other, at the top and bottom tube sides, respectively. The correspondent spin-polarized conductances P_y are shown in Fig. 6 (a). Again, for all cases we get a peak of the absolute value of P_y close to energies $\pm 0.2\,\gamma_0$. It is noteworthy that P_y changes depending on the relative position of the H-adatoms in the unit slab L_0. For case 2 the width of spin-polarization P_y peak shrinks and exhibits an interesting peak inversion compared with case 1, as can be clearly seen in the figure. For the symmetric case 3, the polarization completely disappears in the region corresponding to the first conductance plateau, identical to the results obtained for the pristine case.

To gain some insight on the main different features related to the relative position of the adatoms, we also resort to the band structures of infinite (6,6) CNTs with equivalent defect distributions and the spin polarization $\langle S_y \rangle$ of the states in the bands, for the three cases. The results are depicted in Fig. 6 (b) and clearly show basic differences. In case 1 the bands show large anticrossings at Γ around the energies $\pm 0.2\,\gamma_0$, thus leaving the channels with positive $\langle S_y \rangle$, near X and X', uncompensated. Case 2 shows the opposite behavior: the anticrossings take place near X and X' points, so the remaining channels close to Γ have a negative spin projection $\langle S_y \rangle$. As a result, in case 2 the dominant spin polarization has an inverted sign compared to case 1. In the symmetric case 3, polarizations and slopes of the bands are completely compensated and cancel the net effect, because there are no anticrossings nor band openings at these energies, despite the fact that the bands show net spin values.

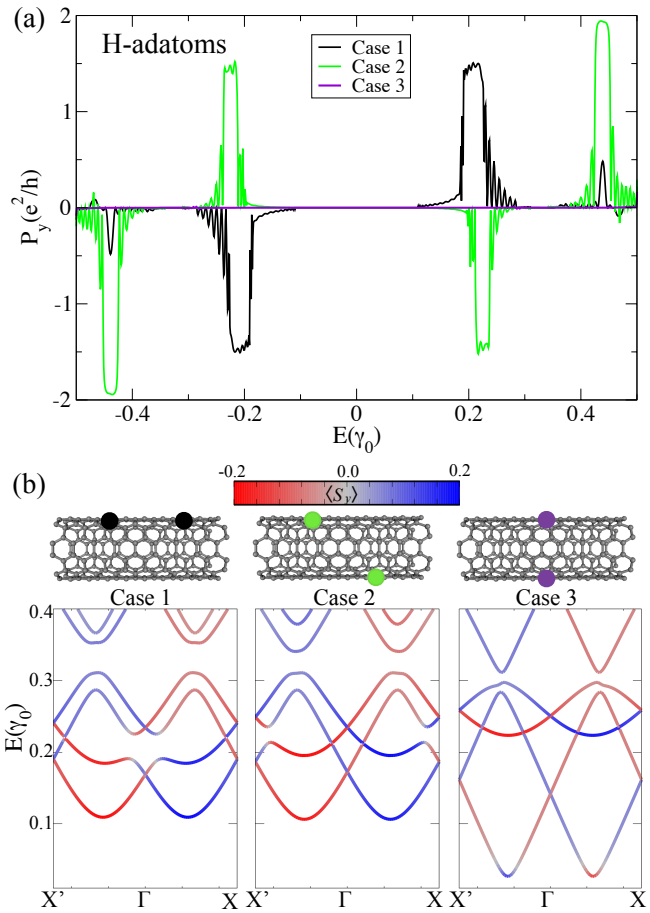

FIG. 6. (Color online) (a) Spin-polarization P_y for a $(6,6)$ CNT with a Rashba region of length $20\,L_0$ ($L_0 = 9T \approx 2.21$ nm) with two H-adatoms in L_0. Three configurations with different relative positions between the adatoms are presented within the L_0 length unit, as detailed in the scheme; the colored dots indicate the H-adatom positions. (b) Electronic band structures for the three cases, together with the spin values of the $\langle S_y \rangle$ at the adatoms, as defined in Fig. 1, in color resolution (blue for up spin and red for down spin).

These results can be of practical interest. The fact that adatoms situated in the same side of the tube give rise to spin-polarized currents that present inverted polarization signals when the H-adatoms are situated in opposite sides (top and bottom sides of the tube), may be of great importance, for instance, for transport and storage spin-information. Actually, DNA wrapped around single-walled carbon nanotubes are shown to induce helicoidal electric field by the polar nature of the adsorbed DNA molecule [23] and spin polarized currents are produced depending on the molecular hybrid system configurations. Our results show that it could be possible to engineer particular defect configurations on the CNTs

(decorated-like tube) opening new routes for their use in spintronic devices [28].

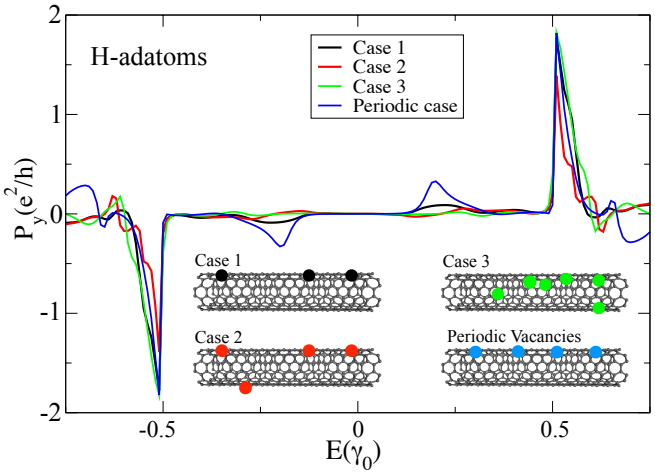

FIG. 7. (Color online) Spin-polarization P_y for a $(6,6)$ CNT with a Rashba region composed of 16 unit cells ($L = 16\,T$) for the H-adatoms distributions given in the inserts.

D. Non equal spaced distribution of H-adatoms

Finally, in order to extend our analysis beyond periodic configurations of defects, we have also considered several non equally spaced H-adatom distributions within the Rashba region (see the inserts in Fig. 7). In cases 1 and 2 we have three and four H-adatoms in top and bottom positions with non equal spacing, respectively. Seven adatoms at random positions have been used in case 3. Four equally-spaced H-adatoms have also been calculated for comparison. In all cases, the length of the Rashba region is taken as $L = 16\,T \approx 3.94$ nm.

Fig. 7 shows P_y for these different adatom distributions. We see that the energy values of the peaks of the spin-polarized conductances are robust, maintaining almost the same position for all the H-adatom distributions: the peaks appear next to the energy values of the spin-polarized conductance peaks exhibited for the equally spaced case. But for cases 1 to 3 the height of those peaks closer to the Fermi energy clearly is clearly smaller than for the equally spaced defects. Therefore, it appears that the best scenario to obtain spin-polarized conductances in these CNTs is when the H-adatoms are equally spaced within the Rashba region.

IV. SUMMARY

We have presented a detailed study of the effects of H-adatom and Stone-Wales defects on the spin-polarized currents induced by a RSO interaction in metallic carbon nanotubes. Our main results show that (i) defects provide an increase of the spin-polarized currents at energies close to the Fermi energy; (ii) the spin-polarized currents appear when an imbalance between spin-polarized states with the same slope emerges in the system, and furthermore (iii) such currents are greatly enhanced when the defects are introduced in the system with equally spaced distances. Actually, a single defect scenario appears to be insufficient to generate significant spin-dependent currents, but adding a few equispaced defects yields a relevant result. In turn, equally spaced defects in the Rashba region are found to be the most favorable configuration for the obtention of spin-polarized currents in carbon materials, although random H-adatoms do produce polarization signatures.

We have also found the relevance of the orientation of the defects respect to the direction of the electric field that causes the RSO interaction. Specifically, we have observed that a change in the relative position of neighbor defects (from top-top to top-bottom) has arisen as a switch for a peak inversion of the spin polarization P_y. These results can be useful for defining new routes in the design of spintronic devices with defected CNTs.

V. ACKNOWLEDGMENTS

A. L. acknowledges the financial support of FAPERJ through grant E-26/102.272/2013, CNPq and INCT em Nanomateriais de Carbono. L. C. acknowledges support from Spanish MINECO through Grant FIS2015-64654-P, and helpful conversations with Jorge I. Cerdá. H. S. is grateful for financial support from the Brazilian CAPES (Coordenação de Aperfeiçoamento de Pessoal de Nível Superior, fundação do Ministério da Educação).

[1] J. Padilha, R. Amorim, A. Rocha, A. da Silva, and A. Fazzio, Solid State Communications, **151**, 482 (2011).
[2] K. M. McCreary, A. G. Swartz, W. Han, J. Fabian, and R. K. Kawakami, Phys. Rev. Lett., **109**, 186604 (2012).
[3] M. M. Ugeda, I. Brihuega, F. Guinea, and J. M. Gómez-Rodríguez, Phys. Rev. Lett., **104**, 096804 (2010).
[4] H. González-Herrero, J. M. Gómez-Rodríguez, P. Mallet, M. Moaied, J. J. Palacios, C. Salgado, M. M. Ugeda, J.-Y. Veuillen, F. Yndurain, and I. Brihuega, Science, **352**, 437 (2016), ISSN 0036-8075.
[5] J. R. Sanchez-Valencia, T. Dienel, O. Groning, I. Shorubalko, A. Mueller, M. Jansen, K. Amsharov, P. Ruffieux, and R. Fasel, Nature, **512**, 61 (2014).
[6] P. Ruffieux, S. Wang, B. Yang, C. Sánchez-Sánchez, J. Liu, T. Dienel, L. Talirz, P. Shinde, C. A. Pignedoli, D. Passerone, T. Dumslaff, X. Feng, K. Müllen, and

R. Fasel, Nature, **531**, 489 (2016).
[7] L. Chico, A. Latgé, and L. Brey, Phys. Chem. Chem. Phys., **17**, 16469 (2015).
[8] H. Santos, A. Latgé, J. E. Alvarellos, and L. Chico, Phys. Rev. B, **93**, 165424 (2016).
[9] E. H. Lieb, Phys. Rev. Lett., **62**, 1201 (1989).
[10] S. Saremi, Phys. Rev. B, **76**, 184430 (2007).
[11] J. J. Palacios, J. Fernández-Rossier, and L. Brey, Phys. Rev. B, **77**, 195428 (2008).
[12] H. Santos, D. Soriano, and J. J. Palacios, Phys. Rev. B, **89**, 195416 (2014).
[13] S.-Z. Liang and J. O. Sofo, Phys. Rev. Lett., **109**, 256601 (2012).
[14] R. Saito, M. Fujita, G. Dresselhaus, and M. Dresselhaus, Appl. Phys. Lett., **60**, 2204 (1992).
[15] L. Chico, V. H. Crespi, L. X. Benedict, S. G. Louie, and M. L. Cohen, Phys. Rev. Lett., **76**, 971 (1996).
[16] J.-C. Charlier, T. W. Ebbesen, and P. Lambin, Phys. Rev. B, **53**, 11108 (1996).
[17] Z. Qiao, S. A. Yang, W. Feng, W. K. Tse, J. Ding, Y. Yao, J. Wang, and Q. Niu, Phys. Rev. B, **82**, 161414 (2010).
[18] L. Lenz, D. F. Urban, and D. Bercioux, Eur. Phys. J. B, **86**, 502 (2013).
[19] D. Marchenko, A. Varykhalov, M. R. Scholz, G. Bihlmayer, E. I. Rashba, A. Rybkin, A. M. Shikin, and O. Rader, Nat. Commun., **3**, 1232 (2012).
[20] J. Balakrishnan, G. K. W. Koon, A. Avsar, Y. Ho, J. H. Lee, M. Jaiswal, S.-J. Baeck, J.-H. Ahn, A. Ferreira, M. A. Cazalilla, A. H. Castro Neto, and B. Özyilmaz, Nat. Commun., **5**, 4748 (2014).
[21] R.Winkler, *Spin-Orbit Coupling Effects in Two-Dimensional Electron and Hole Systems* (Springer-Verlag Berlin, 2003).
[22] F. Xu, B. Li, H. Pan, and J.-L. Zhu, Phys. Rev. B, **75**, 085431 (2007).
[23] G. S. Diniz, A. Latgé, and S. E. Ulloa, Phys. Rev. Lett., **108**, 126601 (2012).
[24] F. Zhai and H. Q. Xu, Phys. Rev. Lett., **94**, 246601 (2005).
[25] P. L. McEuen, D. H. Bockrath, M. Cobden, Y.-G. Yoon, and S. G. Louie, Phys. Rev. Lett., **83**, 5098 (1999).
[26] S.Datta, *Electronic Transport in Mesoscopic Systems* (Cambridge University Press, 1997).
[27] H. Santos, L. Chico, and L. Brey, Phys. Rev. Lett., **103**, 086801 (2009).
[28] K. M. Alam and S. Pramanik, Adv. Funct. Mater., **25**, 1616 (2015).